Analysis of active earth pressure behind rigid retaining walls considering curved slip surface

Pengqiang Yu (yu_pengqiang@163.com)
University of Science and Technology Beijing https://orcid.org/0000-0002-0317-4749
Yang Liu
University of Science and Technology Beijing

Research Article

Keywords: earth pressure, soil arching effects, two-dimensional analysis, sandy backfill, curved slip surface

Posted Date: May 16th, 2022

DOI: https://doi.org/10.21203/rs.3.rs-370995/v1

Analysis of active earth pressure behind rigid retaining walls considering curved slip surface

Pengqiang Yu*, Yang Liu

Pengqiang Yu*
Department of Civil Engineering, University of Science and Technology Beijing, Beijing 100083, China
E-mail: yu_pengqiang@163.com
Yang Liu
Department of Civil Engineering, University of Science and Technology Beijing, Beijing 100083, China

Abstract The active earth pressure acting on the rigid vertical retaining walls under translation mode has been investigated in this paper with a two-dimensional analytical method without prior hypotheses of the shape of soil arch, i.e. the trajectory of minor principle stress, which is totally different from with the existing method of combination of soil arch shape and horizontal flat-element analysis. Different emerging failure surface was compared and a parabolic surface was especially discussed in details. The proposed formula can be employed to predict the distribution of earth pressure and stresses in the failure zone. Furthermore, the analytical expression of the minor principle stress trajectory in the failure zone was derived from the stress equations. The results of the proposed analysis were compared with test data as well as the results of existing theories to validate its accuracy and applicability. The proposed distribution of earth pressure is in good agreement with the test data. Finally, a simple yet practical formulation was established to conveniently estimate active earth pressure in field.

Keywords: earth pressure; soil arching effects; two-dimensional analysis; sandy backfill; curved slip surface

Declarations

Funding: This research was funded by the financial support of the National Natural Science Foundation of China (51178044).
Conflict of interest: The authors declare no conflict of interest.

1 INTRODUCTION

A precise prediction of active earth pressure against the retaining structure is an essential issue in geotechnical engineering. Conventionally, the classical Rankine and Coulomb theories with a simple linear distribution of earth pressure have been widely used in field. However, numerous experimental studies[1-5] show the nonlinear distribution of earth pressure associated with soil arching effects. Numerical simulations, a supplementary tool to investigate the interaction of soils and walls, also indicate that the nonlinearity of active earth pressure distribution behind the retaining wall exists. For example, Benmeddour [6] estimated the earth pressure coefficients with finite difference methods, considering the effects of soil-wall friction angle, backfill inclination and proximity of a slope. Other researchers [7, 8] conducted three-dimensional numerical simulations to investigate earth pressure on a rigid rough retaining wall.

Because of the contradiction between classical theoretical analysis and experimental and numerical results, a growing number of researchers have attempted to establish formulations reflecting nonlinear distribution of earth pressure. Usually, theoretical analysis can be classified into three groups, i.e., slip line method, limit analysis and limit equilibrium method. Among these three methods, the limit equilibrium method is practically commonly used. The appearance of the horizontal flat-element method, which could describe the nonlinearity of active earth pressure distribution, is a key milestone for the theoretical analysis of earth pressure. After that, numerous studies[9-13] on the active earth pressure based on the horizontal flat-element method were conducted from various perspectives, e.g. the modes of wall movement, seismic earth pressure, cohesive backfill and so forth. Yet, soil arching effect, a common phenomenon in geotechnical engineering,

was not involved in the above studies. Terzaghi[14] and Han[15] confirmed the existence of soil arching in soils using trap door experiments.

Handy[16] suggested that the influence of soil arching effects on the nonlinear distribution of earth pressure not be neglected. He proposed a formula for estimating the active earth pressure acting on rigid walls under assumptions of the plane slip surface and the catenary minor principal stress trajectory (arching shape). Later, several researchers[17,18] also investigated active earth pressure taking into account soil arching effects by means of minor principal stress trajectory. Paik[17] originally attempted to incorporate the trajectory of minor principal stress to the horizontal flat-element method in the investigation of active earth pressure against rigid retaining walls. Since then, the method of combining stress trajectory with differential flat- elements in a wedge-shaped failure zone to investigate earth pressure exerting on rigid retaining walls attracted many researchers' attention and they also presented various formulations to evaluate active earth pressure based on different assumptions of stress trajectory (e.g. arc, parabola or catenary) and the inclination of plane slip surface(e.g. Rankine or Coulomb slip surface)[18-22], except for a parabolic slip surface used by Geol[23].

Hitherto, most of the existing arching-considered formulations to estimate active earth pressure were established by incoporating minor principal stress trajectory into differential flat-element method. These formulations can only discribe the earth pressure distribution along the wall, but the stress state in the failure zone behind the wall still remains unknown. Besides, the above methods implicitly assume that arbitrary soil element in the failure zone yielded, not only in the slip surface and adjacent the wall, which is contradicted with the actual situation. The simplification of only focusing on average vertical pressure and ignoring shear force between flat elements results in force unbalance in the horizontal direction. The earth pressure distribution in this method depends on the assumpotion of minor principal stress trajectory, but the difference between hypothetical and real stress trajectories has not been validated.

It is noted that the shape of slip surface has a great influence on the determination of active earth pressure. There are two types of common slip surface developed in the backfill, i.e., plane and curve surface. Generally, the plane slip surfaces include Rankine slip surface, a plane inclining at an angle of $\pi/4+\varphi/2$ to the horizontals, and Coulomb slip surface, a plane inclining at an angle of β to the horizontals, where the angle of β is derived from Coulomb theories. The Rankine slip surface only exists when the wall is smooth where the soil-wall friction angle equals zero. As for a rigid rough wall, the slip surface depends on the mode of wall movement and soil–wall friction angle, for instance, Coulomb slip surface. On the other hand, it is widely accepted that the slip surface that develops in the retained soil under active condition tend to be curved. However, due to the complexity of analytical derivation on curve surface, studies adopting curve slip surface are rare in estimating earth pressure.

From the above, there are several shortconmings in existing arching-based formulations to estimate active earth pressure: (1) the trajectory of minor principal stress is previously assumed; (2) they can only obtain the earth pressure against the wall, but the stress distribution in the backfill is unclear; (3) the flat element only satisfies equilibrium in vertical direction; (4) the slip surface in the backfill is commenly regarded as plane, not curved. The present paper attempt to investigate the problem of active retaining walls in a bidirectional balancing system without any assumption about stress trajectory.

Janssen[24] proposed an analytical expression for the pressure acting on the silo under the assumption of uniform vertical stress in a horizontal plane, which yielded satisfactory results. Similarly, Jaky[25] invetsigated the silo problem by assuming that the shear stress experienced a linear decrease at a certain depth, which is corresponding to Janssen's hypothesis. In this paper, the issue of active earth pressure against a rigid retaining wall under translation is studied with the same assumption used by Janssen. Based on the force balance of two-dimensional differential element, theoretical stress solutions, i.e. vertical, horizontal and shear stresses, of any point in the failure zone are obtained. Although it is ideal to assume that the vertical stress at a certain depth is uniform, Handy[16] suggested that the vertical stress experienced small fluctuation of only 1% from the wall to slip surface regardless of internal friction angle. Hence, the formulations presented in this paper could be used to estimate the active earth pressure against rigid retaining walls.

Based on the assumption motioned above and reasonable boundary conditions, novel formulations of stress condition at any point within the parabolic slip surface are derived by solving the 2D equilibrium equa-

tions of a differential element. Meanwhile, the stress solutions under two typical plane slip surfaces with the same assumption are also derived to discuss the influence of slip surface. Furthermore, the trajectories of minor principle stress can be easily obtained according to the obtained stress solutions; therefore, the soil arching effects in the backfill behind a retaining wall can be depicted theoretically. A series of parametric analysis have been also conducted and some conclusions were drawn simultaneously. Finally, comparisons are made with the results obtained from the existing theories and experimental data. It should be noted that the presented method only considered the stress balances like other limiting equilibrium method, ignoring the strain compatibility.

2 THE PROPOSED TWO-DIMENSIONAL ANALYSIS

2.1 Basic Hypotheses

Figure 1 shows the calculation model of active earth pressure on a retaining wall. The basic assumptions are as follows. (1) The retaining wall is vertical and rough. (2) The backfill is an ideal elastic-plastic material that obeys the Mohr–Coulomb yield criterion, and is an isotropic continuous material, represented by two characteric parameters γ and φ. (3) The soil-wall interface satisfies Coulomb's friction law, represented by constant δ. (4) The emerging slip surface in the backfill develops from the bottom of the wall with a planar or curved surface.

2.2 Basic Equations

As illustrated in Figure 1, the origin of rectangular coordinate system is set at the inner bottom of the retaining wall for convenience of analysis. The *x*-axis measures the horizontal distance from the wall and the *z*-axis shows the vertical height to a certain depth. According to the stress condition of the differential element in the failure zone depicted in Fig.1, the static equilibrium equations can be described as

$$\frac{\partial \sigma_x}{\partial x}+\frac{\partial \tau_{zx}}{\partial z}=0 \tag{1}$$

$$\frac{\partial \sigma_z}{\partial z}+\frac{\partial \tau_{xz}}{\partial x}=-\gamma \tag{2}$$

Where σ_z and σ_x are vertical and horizontal normal stress, respectively; τ_{xz} is the shear stress along the horizontal direction, while τ_{xz} is the shear stress along the vertical direction; γ is the unit weight of the backfill. The compressive stresses, to facilitate derivation, are considered as positive in this paper.

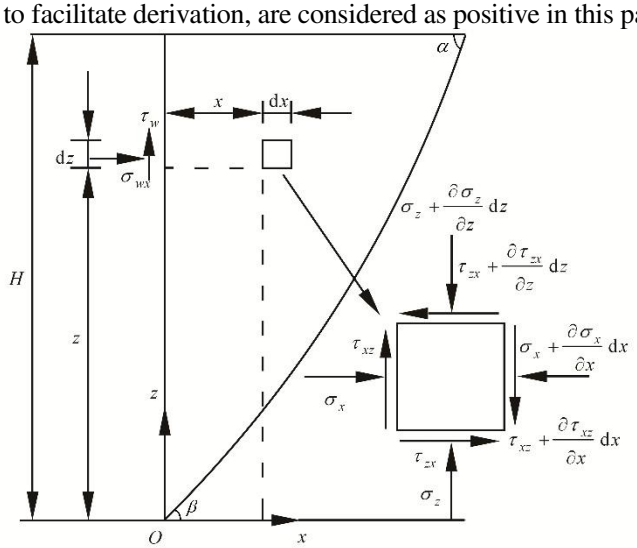

Figure 1: Stress state of a differential element in backfill soil behind a retaining wall under translating mode

2.3 Boundary Condition

To accurately determine the boundary conditions corresponding to the real condition, the mobilizations of the friction angle will be discussed firstly. Mao[26] indicated that it is unlikely that the internal friction angle φ and soil-wall friction angle δ are fully mobilized at the same time. That is to say, the wedge cannot simultaneously slide along two planes, which violate the laws of mechanics. Li et al.[27] revealed that the mobilized soil-wall friction angle stabilizes its maximum value after the wall movement exceeds 0.04%H approximately, while the full mobilization of the internal friction angle requires 0.3%H. Hence, we can assume that the fully mobilization of the soil-wall friction angle precedes that of the internal friction angle. Besides, the results of proposed method under the condition of full mobilization of internal friction angle show that the earth pressure acting on the wall is negative at the upper depth, which means that an early limit state has been appeared because it is impossible to have tensile stress in a friction soil. Therefore, the backfill behind the wall is regarded to have reached the active limit state just when the soil-wall friction angle is fully mobilized in this study.

2.3.1 Stress Boundary Condition on the Soil-Wall Interface

On account to the yielding of the backfill adjacent to the retaining wall, the stress state of which can be expressed by a constant value K_w as follows[18-24]:

$$K_w = \frac{\sigma_{wx}(z)}{\sigma_{wz}(z)} = \frac{1-\cos(\arcsin(\sin\delta/\sin\varphi)-\delta)\sin\varphi}{1+\cos(\arcsin(\sin\delta/\sin\varphi)-\delta)\sin\varphi} \tag{3}$$

Where $\sigma_{wx}(z)$ and $\sigma_{wz}(z)$ are the horizontal and vertical compressive stress adjacent to the wall, respectively; δ is the wall-soil friction angle, and φ is the internal friction angle of the backfill in which $\delta \le \varphi$.

The full mobilization of the wall-soil friction angle indicates that shear stress τ_w along the wall can be calculated by Eq. (4):

$$\tau_w(z) = \mu_w \sigma_{wx}(z) \tag{4}$$

Where $\mu_w = \tan\delta$.

In view of the assumption on vertical stress σ_z of uniform distribution at a certain height, the vertical stress $\sigma_{wz}(z)$ is equal to $\sigma_z(z)$, i.e., $\sigma_{wz}(z) = \sigma_z(z)$. Then, the shear stress τ_w can be rewritten as Eq. (5) by substituting Eq. (3) into Eq. (4):

$$\tau_{xz}(x,z)\big|_{x=0} = \mu_w K_w \sigma_z(z) = A\sigma_z(z) \tag{5}$$

Where $\tau_{xz}(x,z)\big|_{x=0} = \tau_w(z)$, and $A = \mu_w K_w$ is defined as stress coefficient for the convenience of writing and derivation.

2.3.2 Emerging Slip Surface and Stress Boundary Condition

Many experimental studies[28, 29] show a curved failure surface developing in the backfill behind rigid walls. As Spangler and Handy[30] indicated, the shape of emerging failure surface can be defined as a parabolic curve. Soltanbeigi[28] conducted full-scaled physical retaining wall model tests using Particle Image Velocimetry technology and found the active failure surface can be described with a 2nd rank parabolic function. In this study, the parabolic equation is defined as follows:

$$z = ax^2 + bx + c \tag{6}$$

Where *a*, *b*, and *c* are constants, which can be obtained through the following conditions: (1) The failure of the backfill is greatly influenced by the rough wall, so the slope of the failure surface at the bottom of the wall can be considered to be β (Fig.1), i.e., the inclination of plane failure surface from Coulomb theory, which can reflect the impact of soil-wall friction on the failure surface. (2) Whereas, the influence of the soil-wall friction significantly decreases with the distance of wall. Therefore, it is reasonable to assume the failure surface with a slope of $\alpha = \pi/4 + \varphi/2$ near the top, which is consistent with the Rankine theory and Paik's work.

The restrained conditions can then be expressed as follows:

$$\left.\begin{aligned} z=0,\quad & x=0 \\ z=0,\quad & \frac{\mathrm{d}z}{\mathrm{d}x}=\tan\beta \\ z=H,\quad & \frac{\mathrm{d}z}{\mathrm{d}x}=\tan\alpha \end{aligned}\right\} \tag{7}$$

Where $\beta=\arctan(\sqrt{\tan^2\varphi+\tan\varphi/\tan(\varphi+\delta)}+\tan\varphi)$. Thus, these constants can be easily obtained by substituting Eq. (7) into Eq. (6):

$$\left.\begin{aligned} a&=\frac{\tan^2\alpha-\tan^2\beta}{4H} \\ b&=\tan\beta,\ c=0 \end{aligned}\right\} \tag{8}$$

Inserting the obtained constants into Eq. (6), the parabolic equation is rewritten as:

$$z=[(\tan^2\alpha-\tan^2\beta)/4H]x^2+x\tan\beta \tag{9}$$

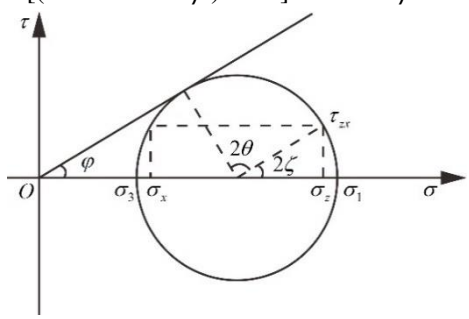

Figure 2: Calculation of the stress ratio B

In some special conditions, *a* will be taken as zero, and a planar failure surface is then obtained, which will be discussed below.

It should be mentioned that although the internal friction angle is not fully mobilized in the backfill, the stress ratio $B=\tau_{xz}(x,z)/\sigma_z(z)$ of the soil element at the failure surface is assumed to be identical to that obtained from the Mohr circle when it yields, as shown in Fig.2.

The following expressions can be gotten from Fig.2,

$$2\zeta=\pi/2+\varphi-2\theta \tag{10}$$

$$B=\frac{\tau_{zx}}{\sigma_z}=\frac{\tau_{xz}}{\sigma_z}=\frac{\sin\varphi\sin 2\zeta}{1+\sin\varphi\cos 2\zeta} \tag{11}$$

Where ζ is the inclination of minor principle stress measured from the horizontals at the state of failure, θ is the angle between the tangent line of failure surface and horizontal direction at *z* depth, $\beta\le\theta\le\alpha$. *B* is the ratio of τ_{xz} and σ_z at the slip surface.

The angle θ can be obtained by differentiating Eq. (9) with respect to *x*:

$$\theta=\arctan(\sqrt{b^2+4az}) \tag{12}$$

Substituting Eq. (10) and Eq. (12) into Eq. (11), *B* can be denoted as the following expression:

$$B=\left.\frac{\tau_{xz}}{\sigma_z}\right|_{x=(\sqrt{b^2+4az}-b)/2a}=\frac{\sin\varphi\sin 2(\pi/2+\varphi-2\arctan(\sqrt{b^2+4az}))}{1+\sin\varphi\cos 2(\pi/2+\varphi-2\arctan(\sqrt{b^2+4az}))} \tag{13}$$

2.4 Solutions of the Equilibrium Equations

According to the assumption that the vertical stress σ_z keeps constant for a given height z within the slip surface, we can easily obtain Eq. (14) after a partial derivative to Eq. (2) with respect to x:

$$\frac{\partial^2 \tau_{xz}}{\partial x^2} = 0 \tag{14}$$

The general solution of Eq. (14) can be expressed as follows:

$$\tau_{xz}(x,z) = C_1(z)x + C_2(z) \tag{15}$$

Where $C_1(z)$ and $C_2(z)$ are integration coefficients depending on z.

Substituting Eq. (5) and Eq. (13), i.e. the boundary conditions of stresses at x=0 and $x = (\sqrt{b^2 + 4az} - b)/2a$, into Eq. (15), the shear stress τ_{xz} is transformed into Eq. (16):

$$\tau_{xz}(x,z) = [\frac{2a(A-B)}{b - \sqrt{b^2 + 4az}} x + A]\sigma_z(z) \tag{16}$$

Eq.(16) shows that the shear stress τ_{xz} at the same depth z makes a constant decrease with the increase of x due to $A > B$, which is consistent with the hypothesis on linearly decreased shear stress from the wall assumed by Jaky[25].

Substitution of Eq. (16) into Eq. (2) yields the following differential equation:

$$\frac{\mathrm{d}\sigma_z}{\mathrm{d}z} + \frac{2a(A-B)}{b - \sqrt{b^2 + 4az}} \sigma_z = -\gamma \tag{17}$$

Although it is unlikely to obtain an analytical solution of the above equation because of complexity, it is convenient to get a numerical solution of σ_z under a given condition of (φ, δ) using mathematical software such as Matlab. Subsequently, τ_{xz} in the sliding backfill behind retaining wall can be obtained in the light of Eq. (16). Finally, the horizontal stress σ_x in the failure zone can be calculated by the following equation:

$$\sigma_x(x,z) = -\int_0^x \frac{\partial \tau_{xz}(t,z)}{\partial z} dt + K_w \sigma_z(z) \tag{18}$$

Where the upper limit of integration x should be in the range of $[0,\ (\sqrt{b^2 + 4az} - b)/2a]$ at a given height z.

2.5 Active Earth Pressure on the Wall

The active horizontal earth pressure σ_{wx} is equal to $\sigma_x(x,z)$ when x=0 for a certain height z, so σ_{wx} can be calculated by the following equation:

$$\sigma_{wx}(z) = \sigma_x(x,z)\big|_{x=0} = K_w \sigma_z \tag{19}$$

The horizontal resultant P_{ah} acting on the wall can be expressed by the following integral:

$$P_{ah} = \int_0^H \sigma_{wx} \mathrm{d}z \tag{20}$$

Remembering that the soil-wall friction angle δ is fully mobilized, we can reasonably obtain the total active resultant P_a acting on the rigid wall by the following expression:

$$P_a = P_{ah} / \cos\delta \tag{21}$$

Further, the height of the point of application of the total resultant from the bottom of the retaining wall can be calculated by Eq. (22):

$$h_a = \frac{\int_0^H \sigma_{wx}(z) z \mathrm{d}z}{P_{ah}} \tag{22}$$

Finally, The coefficient of active earth pressure K_a is then calculated dividing the total active force P_a by $\frac{1}{2}\gamma H^2$ defined in Coulomb theory. Hence, K_a can be expressed as follows:

$$K_a = \frac{2P_a}{\gamma H^2} \tag{23}$$

Unfortunately, the above solutions and expressions can only be solved with numerical methods at a given (φ, δ). To propose a rigorous analytical equation for conveniently estimating the active earth pressure in practice, the parabolic slip surface can be reduced to a plane, as shown in Fig.3.

It is well known that there are two kinds of planes of the failure surface, i.e., Rankine slip surface and Coulomb slip surface, behind the wall commonly used in engineering practice. Four cases are considered here in what follows (see Fig. 3), to make comparisons between solutions from the plane slip surface and more precise solutions developed previously.

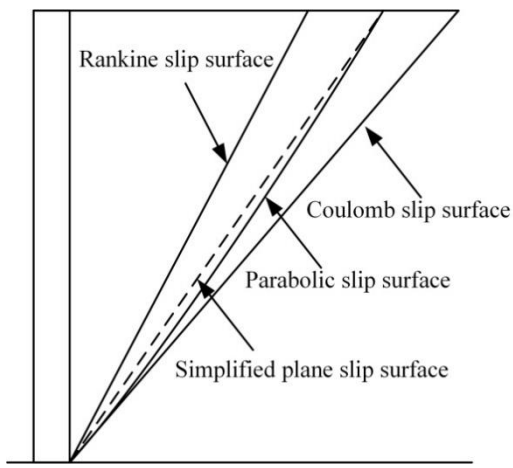

Figure 3: Different emerging failure surfaces for earth pressure calculation

Case 1: General parabolic slip surface, as already discussed above.

Case 2: Coulomb slip surface.

If $\alpha = \beta = \arctan(\sqrt{\tan^2\varphi + \tan\varphi / \tan(\varphi + \delta)} + \tan\varphi)$, the failure surface is simplified to be a plane and identical to the plane determined by Coulomb theory. Consequently, the B in Eq. (13) is transformed into $B = \dfrac{\sin\varphi\sin(\pi/2 + \varphi - 2\beta)}{1 + \sin\varphi\cos(\pi/2 + \varphi - 2\beta)}$, which is taken as a constant independent of z in the case of a given (φ, δ). Therefore, Eq. (17) becomes the following form:

$$\frac{\mathrm{d}\sigma_z}{\mathrm{d}z} - m\frac{\sigma_z}{z} = -\gamma \tag{24}$$

Where $m = (A - B)\tan\beta$, a function of δ and φ.

The general solution of Eq. (24) can then be derived as showed in Eq. (25):

$$\sigma_z(z) = \begin{cases} C_3 z - \gamma z \ln(z) & m = 1 \\ C_4 z^m + \dfrac{\gamma z}{m-1} & m \neq 1 \end{cases} \tag{25}$$

Herein C_3 and C_4 are constants.

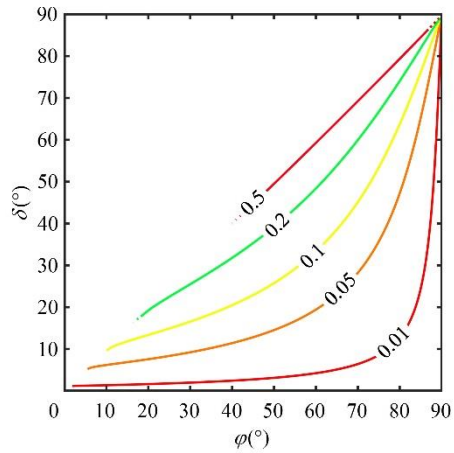

Figure 4: Contour distribution of parameter m

Duo to $m=(A-B)\tan\beta$, the range of m can be illustrated in Fig.4. As shown in Fig.4, the value of m is always less than 1 for all case of (δ, φ). Thus, the condition $m=1$ can be neglected and a particular solution of the expression for $m\neq 1$ is obtained by applying the upper boundary condition at the top layer where the vertical stress is equal to 0:

$$\sigma_z(\mathrm{z})=\frac{\gamma H}{1-m}\left[\left(\frac{z}{H}\right)^m-\frac{z}{H}\right] \tag{26}$$

By replacing the boundary condition $x=(\sqrt{b^2+4az}-b)/2a$ at the failure surface with $x=z\cot\beta$ in Eq. (16), the shear stress τ_{xz} in the sliding zone behind the wall can be obtained after a substitution of Eq. (26) into Eq. (16):

$$\tau_{xz}(x,z)=\frac{\gamma H}{1-m}\left(A-m\frac{x}{z}\right)\left[\left(\frac{z}{H}\right)^m-\frac{z}{H}\right] \tag{27}$$

Substituting Eq. (27) into Eq. (18), the horizontal stress of the backfill behind the wall can be calculated as:

$$\sigma_x(x,z)=\left(K_w-Am\frac{x}{z}+\frac{m(m\text{-}1)}{2}\left(\frac{x}{z}\right)^2\right)\sigma_z(z)+A\gamma x-\frac{m\gamma x^2}{2z} \tag{28}$$

Substituting Eq. (26) into Eq. (19), the lateral active earth pressure acting on the retaining wall under the assumption of Coulomb's failure surface ($\alpha=\beta=\arctan(\sqrt{\tan^2\varphi+\tan\varphi/\tan(\varphi+\delta)}+\tan\varphi)$) can be written as:

$$\sigma_{wx}(z)=\frac{K_w\gamma H}{1-m}\left[\left(\frac{z}{H}\right)^m-\frac{z}{H}\right] \tag{29}$$

The total active resultant acting on the rigid wall P_a can also be derived by substituting Eq. (20) and Eq. (29) into Eq. (21):

$$P_a=\frac{K_w}{(m+1)\cos\delta}\frac{1}{2}\gamma H^2 \tag{30}$$

And the horizontal active force P_{ah} can be derived from Eq. (21):

$$P_{ah}=\frac{K_w}{(m+1)}\frac{1}{2}\gamma H^2 \tag{31}$$

The height h_a of the total resultant from the bottom of the retaining wall is expressed in following equation by substituting Eq. (31) and Eq. (29) into Eq. (22):

$$h_a = \frac{2(m+1)}{3(m+2)} H \tag{32}$$

Finally, the coefficient of active earth pressure K_a can then be obtained as follows:

$$K_a = \frac{K_w}{(m+1)\cos\delta} \tag{33}$$

Case 3: Rankine slip surface.

If $\beta = \alpha = \pi/4 + \varphi/2$, the curved surface is transformed to is a plane with an angle of $\pi/4 + \varphi/2$ from the horizontals, i.e. the Rankine slip surface. Although it only exists when the retaining wall is smooth, it is commonly used in practice for simplicity and practicability. Under this condition, the *B* in Eq. (13) becomes a constant value 0. Substituting $B = 0$ and $\beta = \alpha = \pi/4 + \varphi/2$ into Eq. (24)-Eq. (33), the corresponding solutions under the assumption of Rankine slip surface can be obtained respectively, which is equal to the formulations derived by Khosravi [31]. It is obvious that the solutions in Rankine slip surface are only a special case of that in Coulomb slip surface when the wall is smooth.

Case 4: A simplified plane slip surface.

A simplified plane slip surface can be obtained by linking the two endpoints of the curve slip surface to get an analytical solution to active earth pressure for engineering applications, since the parabolic surface is relatively close to be a plane. The inclination of the simplified plane can be easily calculated as $\varepsilon = \tan^{-1}((\tan\alpha + \tan\beta)/2)$. Lying between the above two planes, it can reflect not only the influence of wall-soil friction in the sub-soil, which is associated with Coulomb slip surface; but the failure of the soil itself associated with Rankine slip surface in the upper soil as well. Thus, the simplified plane should be able to represent the actual condition in the backfill behind the wall at active state. Substituting $\beta = \varepsilon = \tan^{-1}((\tan\alpha + \tan\beta)/2)$ into Eq. (24)-Eq. (33), the corresponding solutions can then be obtained, and the detailed expressions are listed in **section 6** as a practical earth pressure calculation method.

2.6 Comparison of the Solutions from Different Failure Surfaces

Solutions from different failure surfaces are compared here to analyze their differences and similarities. Fig.5 shows the stress distribution normalized by γH in the failure zone derived from the curved failure surface when $\varphi = \delta = 40°$. For clarity, solutions obtained from the curved failure surface were only plotted in Fig. 5.

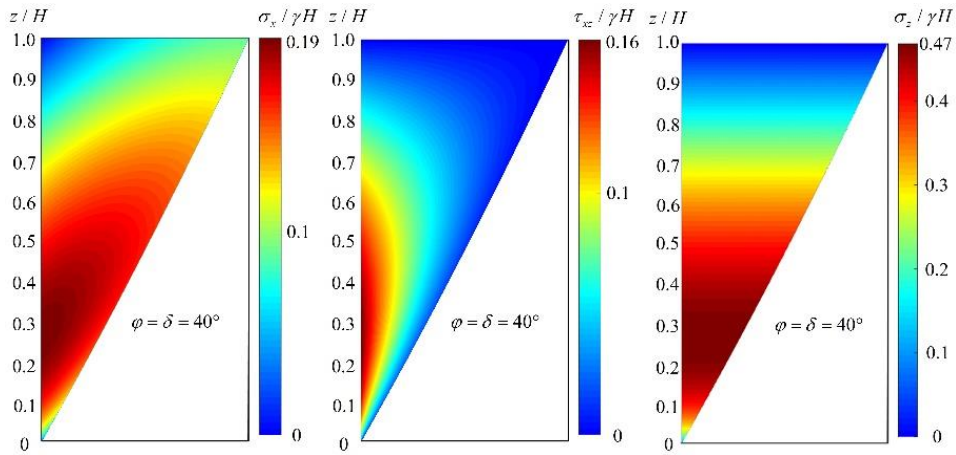

(a) Horizontal stress **(b)** Shear stress **(c)** Vertical stress

Figure 5: Distribution modes of the stresses in the failure zone from the curved failure surface

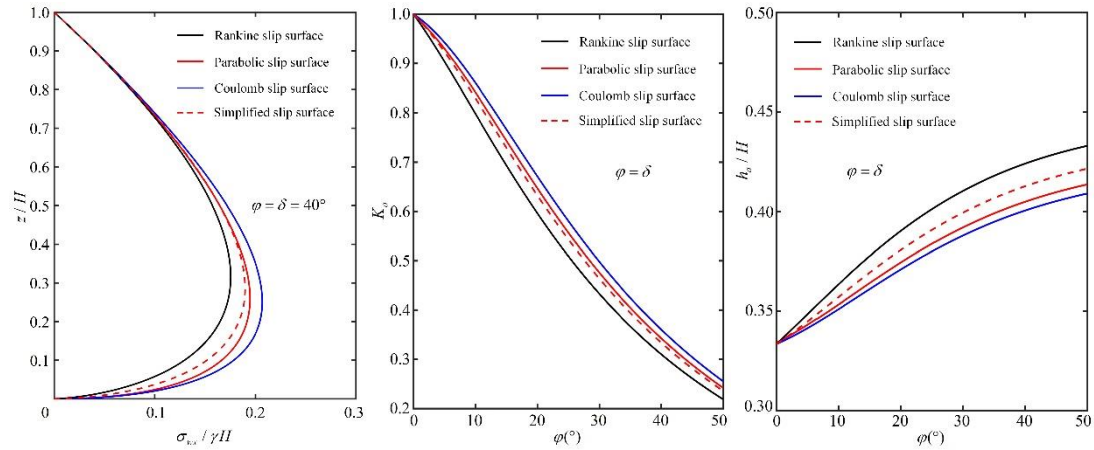

(a) Lateral active earth pressures **(b)** Active earth pressure coefficient K_a **(c)** Height of the application point h_a

Figure 6: Comparisons of active earth pressure for four cases ($\varphi = \delta$)

The distribution patterns of the normalized stresses in the failure zone from the curved failure surface are practically similar to that derived from the plane slip surfaces, but the stress magnitudes obtained from these four cases differ from each other. The stress solutions in the failure zone derived from the parabolic failure surface lie between the solutions obtained from Rankine surface and Coulomb surface. As shown in Fig.5, the shear stress at a given height z constantly reduces with *x*, which is consistent with the previous analysis. The maximum of vertical stress does not occur at the base of the wall, which implies that the soil arching effect exists in the backfill behind the retaining wall.

Fig.6 (a) shows the distributions of the lateral active earth pressure acting on the retaining wall obtained from above four cases. The stresses along the wall are normalized by γH and the depth z are normalized by *H*. The lateral earth pressures are nearly equal in the upper part of the wall. Fig.6 (b) and (c) shows the differences of K_a and h_a for the different slip surfaces, respectively.

One can see from Fig.6 (b) that all of the obtained K_a decrease from 1.0 with the increasing of the internal friction angle, while the h_a increases nonlinearly from 1/3*H* as the internal friction angle increases from 0 to 50°. The K_a obtained from the assumption of parabolic slip surface is always slightly smaller than that of Coulomb slip surface, but greater than that of Rankine slip surface except for the same starting point at $\varphi = 0$; the h_a obtained from the curved slip surface is higher than that of Coulomb slip surface, while it is lower than that of Rankine slip surface.

Nevertheless, the differences origin from different slip surfaces is relatively modest. In the follows, detailed analysis is made on the results with respect to a parabolic slip surface.

3 ANALYSIS OF SOIL ARCH IN THE BACKFILL BEHIND THE WALL

3.1 The Shape of the Soil Arch

The arch shape behind the retaining wall can be represented by the trajectory of minor principle stress of the soil in active state introduced by Handy [16]. The arch shape in failure backfill behind the wall has been inferred and assumed to be arc, parabola and catenary in the horizontal flat-element method [17-20]. In this paper, however, the soil arch shape can be theoretically derived from the stress solutions expressed in Eq. (16), (17) and (18) without any hypothesis. The detailed derivation for the shape of soil arch in the sliding backfill is presented in this section.

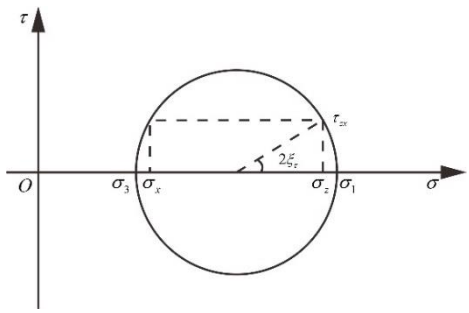

Figure 7: Mohr's stress circle at any point in the sliding backfill

The stress state at any point in backfill under active state condition can be analyzed with Mohr stress circle as shown in Fig.7. The following relationship can be obtained from Fig.7.

$$\tan 2\xi_\tau = \frac{2\tau_{zx}}{\sigma_z - \sigma_x} = \frac{2\tau_{xz}}{\sigma_z - \sigma_x} \tag{34}$$

Where ξ_τ is the angle between the minor principle stress and the horizontals.

Based on the definition of soil arching introduced by Handy, the tangential direction of soil arching curve is the direction of minor principal stress in active state. Therefore, the first derivative of the arching curve with respect to x is equal to $\tan(-\xi_\tau)$. The negative sign means the curve is concave-down. Symbol $f_{arch}(x)$ is introduced to denote the function of soil arching curve at a given height z. Consequently, the first derivative of the arching curve can be expressed as follows:

$$f_{arch}'(x) = \tan(-\xi_\tau) = \tan(\frac{1}{2}\arctan(\frac{2\tau_{xz}}{\sigma_x - \sigma_z})) \tag{35}$$

The analytical expression of soil arching curve at any z can be then obtained by integrating Eq. (35) with respect to x:

$$f_{arch}(x) = \int_0^x \tan(\frac{1}{2}\arctan(\frac{2\tau_{xz}}{\sigma_x - \sigma_z}))dx + z \tag{36}$$

Note that x belongs to the range of $0 \le x \le (\sqrt{b^2 + 4az} - b)/2a$. Substituting the obtained stress solutions in Eq. (16), (17) and (18) into Eq. (36), the shape of soil arch can be clearly showed as in Fig.8 with $\varphi = \delta = 40°$ and $H = 4\text{m}$. The inclination of each arching curve is equal to each other at *x*=0 because of the full mobilization of wall-soil friction angle, but it varies along the slip surface.

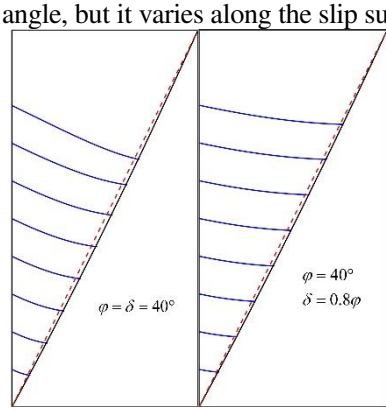

(a) $\varphi = \delta = 40°$ **(b)** $\varphi = 40°, \delta = 0.8\varphi$

Figure 8: Soil arching shape in the failure backfill

3.2 Comparative Analysis of Soil Arch with Other Theories

Fig.9 shows the obtained soil arching shape compared with two other shapes, i.e., circular arc assumed by Liu[19] and parabolic curve assumed by Zhou[18], where the internal frictional angle of the retained soil is determined as φ=40° . Soil arching curves are drawn at $z = 0.4H$ with different soil-wall friction angle δ and the curves are normalized by L in the horizontal and vertical directions for convenience, where L are identical to the horizontal distance from the wall to slip surface at $z = 0.4H$ calculated from the corresponding methods, respectively. The point ($z = 0.4H$, $x = 0$) on the wall is arranged as the origin of coordinates.

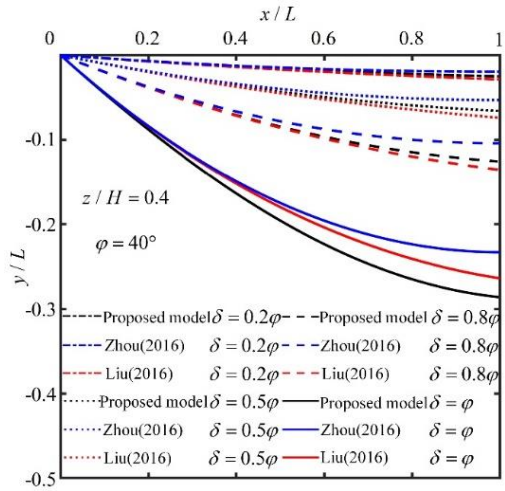

Figure 9: Comparison of soil arching shape from different methods

One can clearly see from Fig.9 that the three types of soil arch are all increasingly steep as the soil-wall friction angle δ grows, which indicates that the soil arching effect will be enhanced by the increase of δ , accompanied by greater deflection of the principle stresses. Although the inclinations of soil arching curves at x=0 in three methods are equal, the differences of soil arching curves for a given δ gradually appear as the distance from the wall increases. The greater soil-wall friction angle δ , the larger the differences.

The developed soil arch is fairly close to the circular arch when $\delta \le 0.5\varphi$, but the differences between them are increasingly significant with the increase of δ . Note that there is a mutation that the developed arch becomes steeper than the circular arch when the soil-wall friction angle is equal, or very close, to the internal friction angle. In other words, when the soil-wall friction angle is quite large, the obtained deflection extent of principle stresses of the soil in the failure zone becomes greater than that calculated from the circular arch. Compared with the parabolic arch by Zhou, the obtained soil arch is increasingly steeper with the soil-wall friction angle growing.

4 PARAMETRIC ANALYSIS

4.1 Internal Friction Angle

Fig.10 (a) shows the distributions of the normalized lateral earth pressure σ_{wx} along a 4 m high retaining wall with varied internal friction angle φ . As illustrated in Fig.10(a), it is obvious that the lateral active earth pressure presents a nonlinear distribution regardless of φ except for a linear distribution when φ=0 . Besides, the lateral earth pressure gradually decreases at a given height z with the increase of φ , and the position of the maximum of earth pressure strength increases accordingly.

Fig.10 (b) shows the difference value $\Delta(\sigma_{wx} / \gamma H)$ between solutions obtained from parabolic slip surface (case 1) and the simplified plane slip surface (case 4). One can see from Fig.10 (b) that the differences increase initially with the increasing of φ , then reverse after reaching to the maximum value as φ is about 20^{o} . But these difference values are relatively small for all φ values.

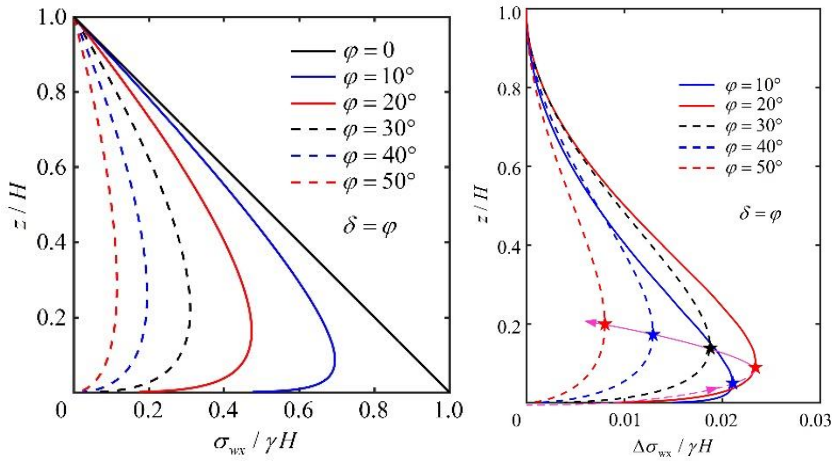

Figure 10: Active Earth pressures **(a)** Distribution varying with φ . **(b)** Difference value from different slip surface

The height of application of the total active resultant normalized by H is drawn as a function of the internal friction angle with different soil-wall friction angle δ in Fig.11. As described in Fig.11, the height of application of the total active resultant maintains a constant of 1/3 in the case of $\delta = 0$, while it experiences a different change when $0 < \delta < \varphi$ and $\delta = \varphi$. In the case of $0 < \delta < \varphi$, with the increasing of internal friction angle, the normalized height increases from a constant of 1/3 to maximum, and then decreases back to 1/3 as φ taken a value of 90° . However, in the particular case of $\delta = \varphi$, the normalized application height increases constantly to a maximum with φ . Furthermore, the influence of φ on the height of application of the active resultant becomes significant with the increase of soil-wall friction angle δ .

It should be noted that the internal friction angle for real soil is usually no higher than 50° , the solutions for cases of internal friction angle higher than 50° have only theoretical meanings.

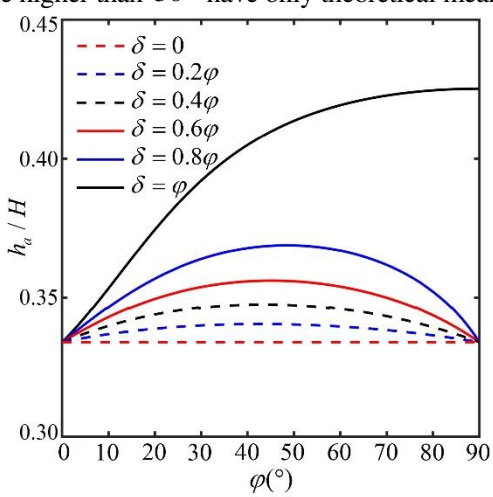

Figure 11: The influence of φ on the height of application of the horizontal active resultant

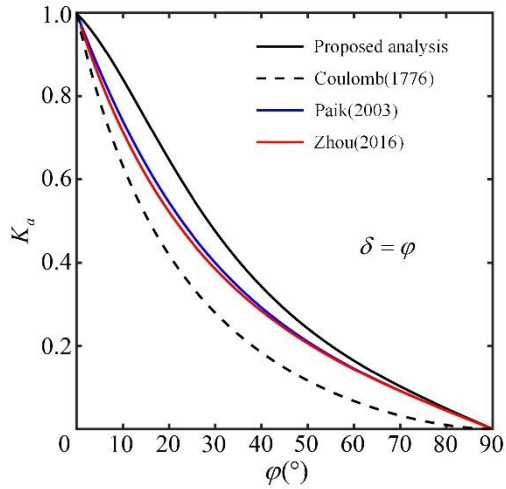

Figure 12: Effect of φ on the coefficient of active earth pressure K_a

Fig.12 shows the variation of the coefficient of active earth pressure K_a with the internal friction angle ranging from 0 to 90° for $\delta = \varphi$. Other results from the equations of Paik[17], Zhou[18] and Coulomb are also plotted in this figure. The coefficients of these four methods all witness a dramatically drop from 1.0 to 0 with the increase of internal friction angle. However, the coefficient K_a from the proposed method is always larger than those of existing theories for $\varphi > 0$. The K_a obtained from Zhou's formulation is roughly the same as that from Paik's theory. They assume the trajectory of minor principle stress as arc and parabolic curves respectively under a same slip plane with the angle of $\pi/4 + \varphi/2$ from the horizontals, i.e. Rankine slip surface, which indicates that the shapes of soil arch have little influence on K_a if a same slip plane is assumed. The K_a obtained from Coulomb's theory is the smallest.

4.2 Soil-Wall Friction Angle

The distribution of lateral earth pressure along the wall, normalized by γH, changing with δ for a given $\varphi = 40°$ is illustrated in Fig.13 (a). One can see from Fig.13 (a) that the earth pressure distribution is linear when $\delta = 0$, which is identical to the result of Rankine theory. While for the case of $\delta \neq 0$, the earth pressure initially increases from 0 and then decreases to 0 along the wall, exhibiting a nonlinear distribution. An intersection point exists between Rankine theory and other cases with $\delta \neq 0$. Furthermore, the lateral active earth pressure above the intersection point gradually increases with the soil-wall friction angle increasing, while decreases below the intersection point for a given internal friction angle φ. This distribution mode enables the height of application of the total active resultant increases as δ increases. Fig.13 (b) shows the difference value $\Delta(\sigma_{wx}/\gamma H)$ between solutions obtained from parabolic slip surface (case 1) and the simplified plane slip surface (case 4). One can see from Fig.13 (b) that the differences increase initially with the increasing of δ; but these difference values are not dramatic for all δ values.

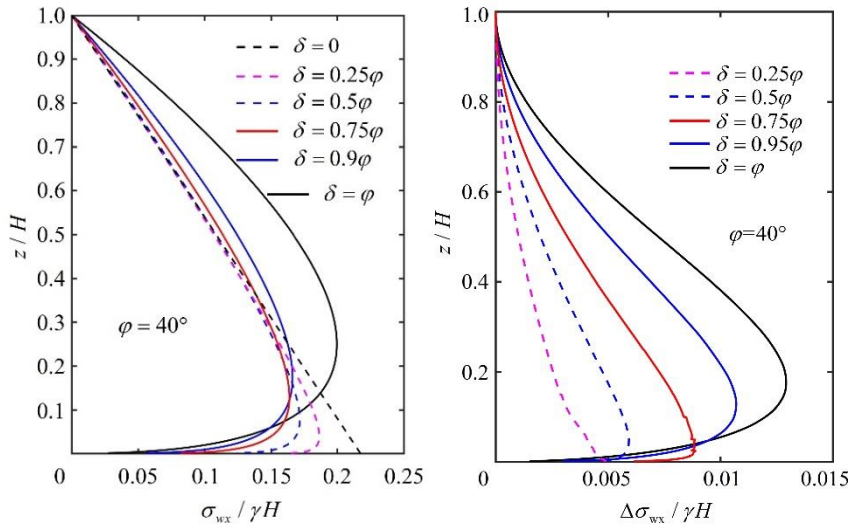

(a) **(b)**

Figure13: Earth pressure distribution **(a)** Distribution variation with δ. **(b)** Difference value from different slip surface

Fig.14 shows the influence of δ on the normalized height of application of the active resultant measured from the bottom of the wall. The results obtained by Paik[17], Zhou[18] and Coulomb are also shown in this figure to make a comparison.

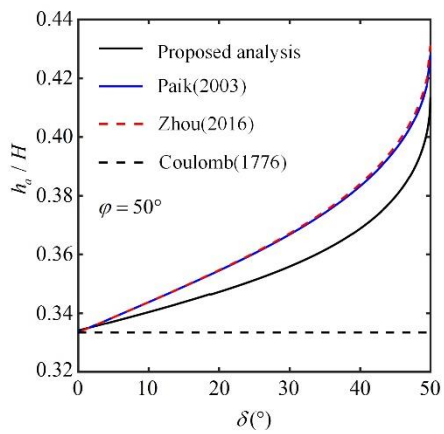

Figure 14: The influence of δ on the height of application of the horizontal active resultant for $\varphi = 50°$

As shown in Fig.14, the normalized height of application of the active resultant calculated from Coulomb theory keeps a constant of 1/3 independent of δ. The results proposed by Paik, Zhou and this paper all increase with the increase of δ. However, the proposed result is smaller than that obtained by Paik and Zhou. Note that, the heights of application of the horizontal active resultant obtained from Paik's and Zhou's formulations are almost the same, which also indicates different assumptions of soil arching shape for a same slip surface have little influence on the height of application of the horizontal active force.

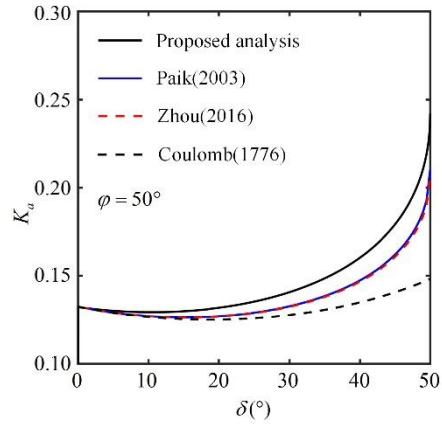

Figure 15: Effect of δ on the coefficient of active earth pressure K_a

Fig.15 plots the change of active earth pressure coefficient K_a with soil-wall friction angle δ from 0 to $50°$ for $\varphi = 50°$. One can see from Fig. 15 that all results have the same trend, i.e. K_a first decreases from the Rankine active earth pressure coefficient at $\delta = 0$ and then increases as the soil-wall friction angle increases. However, the proposed formulation gives the highest active earth pressure coefficient while the Coulomb active earth pressure coefficient is the smallest.

5 COMPARISON WITH EXPERIMENTAL RESULTS

In order to verify the applicability and accuracy, the theoretical predictions of the proposed equations are compared with some experimental data given by Tsagareli[1] as well as the existing theories established by Paik[17], Geol and Patra[23], Handy[16], Zhou[18] and Coulomb.

5.1 Distribution of Active Earth Pressure

Fig.16 shows the comparison on the distributions of lateral active earth pressure between the proposed calculation and other theoretical results motioned above, as well as the experimental data measured by Tsagareli[1].

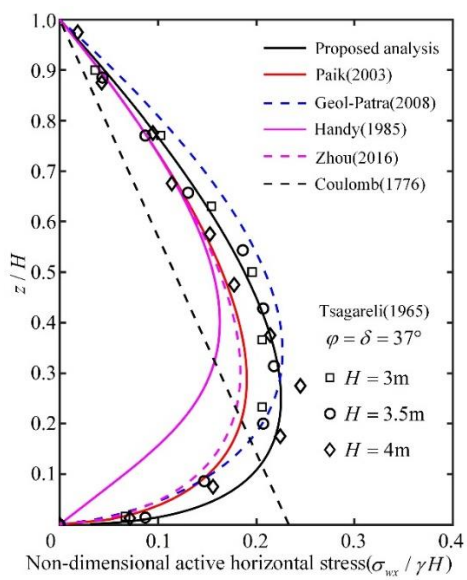

Figure 16: Comparison of the distribution of active earth pressure between theoretical predictions and experimental data

One can see from the figure that the distribution of lateral active earth pressure estimated by the proposed method have a good agreement with the experimental data except for a slightly greater value at the positions

lower than $z/H = 0.2$. Earth pressure calculated from the equations of Handy, Paik and Zhou are close to the experimental data on the top part of the wall but all less than the experimental data on the low part of the wall; while the active earth pressure from Geol's analysis is close to the experimental data on the low part of the wall but higher than the experimental data in the upper part of the wall.

5.2 Magnitude and Height of Application of the Horizontal Active Resultant

The magnitude and height of application point of the horizontal active resultant obtained by different theories and experimental data are plotted in Fig.17 (a) and (b). One can see from Fig.17 (a) that the proposed method gives more accurate predictions for the magnitude of lateral active resultant among all theoretical predictions but a slightly greater value than experimental data. The lateral active resultant calculated by Geol is close to that obtained in this paper, whereas the results provided by other theories give lower values than experimental data.

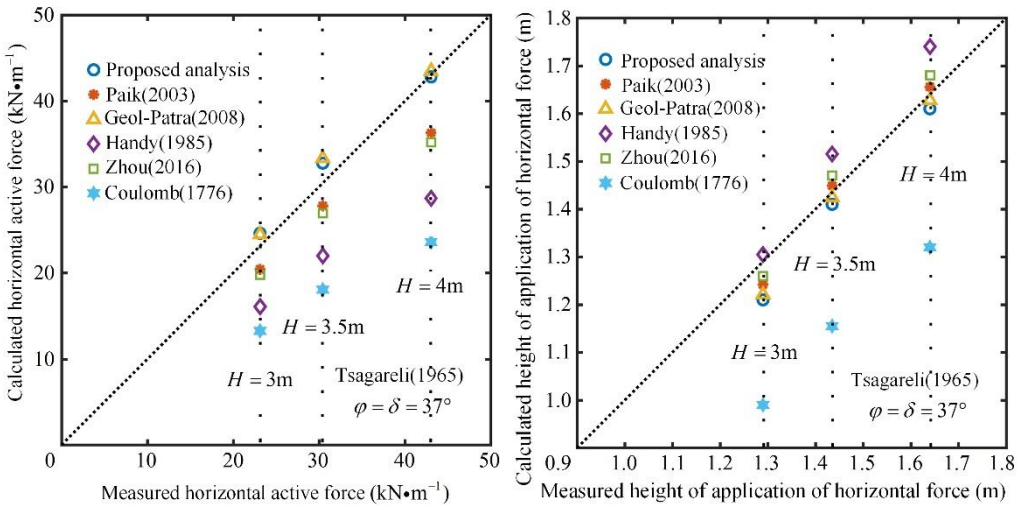

(a) Lateral active force **(b)** Height of application of active force

Figure 17: Comparisons between theoretical predictions and experimental data

Fig.17 (b) shows a comparison of the height of application of the active resultant between the predictions and test data. As shown in Fig.17 (b), Coulomb's solution is usually expressed with respect to the total force and the assumption of a linear active earth pressure distribution gives the lowest values among all theoretical analyses. The proposed method and Geol's theory are all close to the experimental data and give more accurate predictions with the increasing height of wall.

It should be noted that the normalized height of application of the active resultant tends to decrease slightly as the wall height increases according to the experimental results of Tsagareli[1], however, the result calculated from the proposed method is independent of the wall height (Eq.32), in other words, the height of application of the active resultant has a linear relationship with the wall height, which need to be further investigation.

6 PRACTICAL EARTH PRESSURE CALCULATION METHOD

In section 2, the proposed method with 4 different emerging failure surfaces was discussed; but an analytical method cannot be derived directly for the case of a parabolic slip surface; however, an analytical one can be obtained for the simplified slip surface (case 4). The earth pressure solutions obtained from the simplified slip surface are quite close to the solutions from the parabolic slip surface, as well as the experimental data. Hence, it is convenient for engineering applications to use the simplified earth pressure solution. Stresses in the failure zone calculated from the simplified calculation formula are shown in Eq. (37) - (39) as follows,

$$\sigma_z(z) = \frac{\gamma H}{1-m'}\left[\left(\frac{z}{H}\right)^{m'} - \frac{z}{H}\right] \tag{37}$$

$$\tau_{xz}(x,z)=\frac{\gamma H}{1-m'}\left(A-m'\frac{x}{z}\right)\left[\left(\frac{z}{H}\right)^{m'}-\frac{z}{H}\right] \tag{38}$$

$$\sigma_x(x,z)=\left(K_w-Am'\frac{x}{z}+\frac{m'(m'-1)}{2}\left(\frac{x}{z}\right)^2\right)\sigma_z(z)+A\gamma x-\frac{m'\gamma x^2}{2z} \tag{39}$$

Where $m'=(A-B')\tan\varepsilon$, $B'=\dfrac{\sin\varphi\sin(\pi/2+\varphi-2\varepsilon)}{1+\sin\varphi\cos(\pi/2+\varphi-2\varepsilon)}$, and K_w is given in Eq.(3)

The corresponding total active force, coefficient of active earth pressure and the height of the point of application can then be obtained by integrating the stress along the wall as follows,

$$P_a=\frac{K_w}{(m'+1)\cos\delta}\frac{\gamma H^2}{2} \tag{40}$$

$$K_a=\frac{K_w}{(m'+1)\cos\delta} \tag{41}$$

$$h_a=\frac{2(m'+1)}{3(m'+2)}H \tag{42}$$

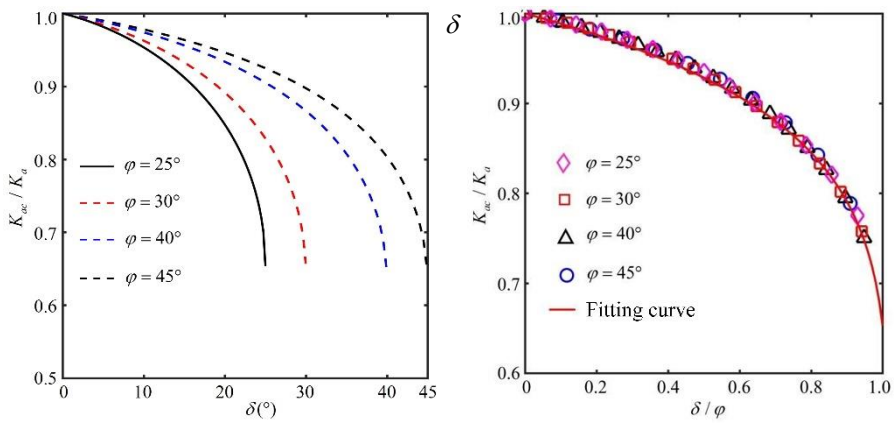

Figure 18: The ratio of K_{ac}/K_a varied **(a)** with soil-wall friction angle and **(b)** with the ratio of δ/φ

One can calculate the earth pressure in practice using Eq. (40)-(42). However, the formula obtained here is still slightly complicated compared with the classical theory such as Rankine or Coulomb. Therefore, it is useful to establish a simple relationship for engineering applications between the obtained active earth pressures and classical theory. To do so, the ratio of the active earth pressure coefficients between the simplified method and Coulomb's theory can be expressed in Eq. (41)

$$\frac{K_{\mathrm{ac}}}{K_a}=\frac{\cos^2\varphi(m'+1)}{K_w\left[1+\sqrt{\dfrac{\sin(\delta+\varphi)\sin\varphi}{\cos\delta}}\right]^2} \tag{43}$$

Where K_{ac} is Coulomb's active earth pressure coefficient and K_a is the pressure coefficient of the simplified calculation method. This relationship is then plotted in Fig. 18(a) with respect to the soil-wall friction angle δ .

One can see from Fig. 18(a) that the ratios decrease continuously from 1 to about 0.65 with the increasing of soil-wall friction angle, no matter how the internal friction angle changes. If the relationship of K_{ac}/K_a is plot in terms of the ratio of δ/φ , as shown in Fig.18(b), four curves in Fig.18(a) become almost coincide with each other and an unique curve can be obtained, which can be described by an exponential function as follows:

$$K_a = (1 - 0.98\delta / \varphi)^{\kappa} K_{ac} \tag{44}$$

Where κ is a coefficient, which is usually taken as a value of -0.11 in practical engineering.

In this way, a simple but practical earth pressure calculation method can be obtained. The design value of active earth pressure can be estimated conveniently using the above formula with the classical Coulomb theory.

7 SUMMARY AND CONCLUSIONS

The active earth pressure acting on the rigid vertical retaining walls under translation mode has been investigated in this paper without prior hypothesis of the shape of soil arch, which is apparently different from the existing methods of combination of soil arch shape and horizontal flat-element analysis. The emerging failure surface was defined as different curves or planes; and a parabolic surface was especially discussed in details. Meanwhile, the simplified analytical solutions under the assumptions of a particular slip surface and solutions with Rankine and Coulomb slip surface are also derived in the same method. The stress solutions of any point in the failure zone is obtained and the active earth pressure acting on the rigid wall is further derived. Furthermore, the analytical expression of trajectory of minor principle stress, i.e. the shape of soil arch, in the failure zone was derived from the stress solutions. Predictions from the proposed method were compared with test data as well as the results of existing theories. Finally, a simple yet practical calculation formulation was proposed to calculate earth pressure in field. Some conclusions can be obtained from this study:

(1) The distribution modes of the normalized stresses in the failure zone with different failure surface are practically identical, but the stress magnitudes differ from each other. The proposed solutions derived from the parabolic failure surface assumption lie between that from Rankine and Coulomb slip surface. The shear stress at a given depth is linearly decreased with the horizontal distance from the retaining wall; the maximum vertical stresses do not appear at the base of the wall, which reflects the effect of soil arching.

(2) The analytical solution of soil arching curve shows it becomes steeper with the increasing of soil-wall friction angle δ. The developed soil arch is fairly close to the circular arch when $\delta \le 0.5\varphi$, however, the differences between them are increasingly significant with the increase of δ, which indicates the assumption of circular shape is rational when δ is small.

(3) The lateral active earth pressure changes from triangular distribution to nonlinear distribution with the increasing of internal friction angle φ. The height of application of the horizontal active force maintains a constant of 1/3 in the case of $\delta = 0$, while it experiences a different change when $\delta > 0$ and $\delta = \varphi$. The distribution of lateral active earth pressure calculated from the proposed method has a good agreement with the experimental data.

(4) The earth pressure solutions obtained from the simplified slip surface are quite close to the solutions from the parabolic slip surface, as well as the experimental data. Hence, it is convenient for engineering applications to use the simplified earth pressure solution. Yet, the practical earth pressure calculation formula related with classical Coulomb theory. i.e., Eq. (44) can also be used to estimate the design value of active earth pressure in filed.

References

[1] Tsagareli, Z. V. (1965). Experimental investigation of the pressure of a loose medium on retaining walls with a vertical back face and horizontal backfill surface. Soil Mech. Found. Eng., ASCE, 2(4), 197-200.

[2] Sherif, M. A. (1984). k_a and k_0 behind rotating and non-yielding walls. J. Geotech. Eng., 110(1), 41-56.

[3] Fang, Y., & Ishibashi, I. (1986). Static earth pressures with various wall movements. J. Geotech. Eng., 120(8), 317-333.

[4] Chang, M. F. (1997). Lateral earth pressures behind rotating walls. Can. Geotech. J, 34(34), 498-509.

[5] O'Nealtroy, S., & Hagerty, D. J. (2011). Earth pressures in confined cohesionless backfill against tall rigid wall. Can. Geotech. J., 48(48), 1188-1197.

[6] Benmeddour, D., Mellas, M., Frank, R., & Mabrouki, A. (2012). Numerical study of passive and active earth pressures of sands. Comput. Geotech., 40(40), 34-44.

[7] Benmebarek, S., Khelifa, T., Benmebarek, N., & Kastner, R. (2008). Numerical evaluation of 3D passive earth pressure coefficients for retaining wall subjected to translation. Comput. Geotech., 35(1), 47-60.

[8] Wörden, F. T., & Achmus, M. (2013). Numerical modeling of three-dimensional active earth pressure acting on rigid walls. Comput. Geotech., 51(2):83-90.

[9] Wang, Y. Z. (2000). Distribution of earth pressure on a retaining wall. Géotechnique, 50(1): 83-88.

[10] Wang, Y. Z., Li, X. G., & Chen, N. N. (2005). Active earth pressure on a retaining wall and lateral coefficient of earth pressure. Rock Soil Mech., 26(7), 1019-1022.

[11] Harrop-Williams, K. O. (1989). Geostatic wall pressures. J. Geotech. Eng., 115(9), 1321-1325.

[12] Lin, Y., Yang, G., Zhao, L., & Zheng, Z. (2010). Horizontal slices analysis method for seismic earth pressure calculation. Chin. J. Rock Mech. Eng., 29(12), 2581-2591.

[13] Lin, Z. Y., Dai, Z. H., & Su, M. X. (2008) Analytical solution of active earth pressure acting on retaining walls under complicated conditions. Chin. J. Geotech. Eng., 30(4), 555-559.

[14] Terzaghi, K. (1943). Theoretical soil mechanics. Wiley, New York.

[15] Han, J., Wang, F., AI-Naddaf, M., & Xu, C. (2017). Progressive development of two-dimensional soil arching with displacement. Int. J. Geomech., 10.1061/(ASCE)GM.1943-5622.0001025, 04017112

[16] Handy, R. L. (1985). The arch in soil arching. J. Geotech. Eng., 111(3), 302-318.

[17] Paik, K. H., & Salgado, R. (2003). Estimation of active earth pressure against rigid retaining walls considering arching effects. Géotechnique, 53(53), 643-653.

[18] Zhou, Y., Chen, Q., Chen, F., Xue, X., & Basack, S. (2018). Active earth pressure on translating rigid retaining structures considering soil arching effect. Eur. J. Environ. Civ. Eng., 22(8), 910-926.

[19] Liu, Z. Y., Chen, J., & LI, D. Y. (2016). Calculation of active earth pressure against rigid retaining wall considering shear stress. Rock Soil Mech., 37(9), 2443-2450.

[20] Rao, P., Chen, Q., Zhou, Y., Nimbalkar, S., & Chiaro, G. (2016). Determination of active earth pressure on rigid retaining wall considering arching effect in cohesive backfill soil. Int. J. Geomech., 10.1061/(ASCE)GM.1943-5622.0000589, 04015082.

[21] Cai, Y., Chen, Q., Zhou, Y., Nimbalkar, S., & Yu, J. (2016). Estimation of Passive Earth Pressure against Rigid Retaining Wall Considering Arching Effect in Cohesive-Frictional Backfill under Translation Mode. Int. J. Geomech., 10.1061/(ASCE)GM.1943-5622.0000786, 04016093.

[22] Chen, J. J., Li, M. G., & Wang, J. H. (2017). Active earth pressure against rigid retaining walls subjected to confined cohesionless soil. Int. J. Geomech., 10.1061/(ASCE)GM.1943-5622.0000855, 06016041.

[23] Goel, S., & Patra, N. R. (2008). Effect of arching on active earth pressure for rigid retaining walls considering translation mode. Int. J. Geomech., 10.1061/(ASCE)1532-3641(2008)8:2(123), 123-133.

[24] Janssen, H. A. (1985). Versuche uber Getreidedruck in silozellen. Z. Ver. Deut. Ingr., 39(35), 1045-1049.

[25] Jaky, J. (1948). Earth pressure in silos, Proc., 2nd Int. Conf. on Soil Mech. Found. Eng., Balkema, Lisse, Netherlands, Vol.1, 103-107.

[26] Mao, Y. S. (1954). Some apparent discrepancies in coulomb's theory and unjustifiable questions about rankine's theory for earth pressure on retaining walls. Chin. Civil Eng. J., 1(3), 249-282.

[27] Li, M. G., Chen, J. J., & Wang, J. H. (2017). Arching effect on lateral pressure of confined granular material: numerical and theoretical analysis. Granular Matter, 19(2):20.

[28] Soltanbeigi, B., Altunbas, A., Gezgin, A. T. & Cinicioglu, O. (2015). Characterization of active failure wedge for cohesionless soils. Eur. Conf. on Soil Mech. Geotech. Eng.

[29] Yang, M., & Tang, X. (2017). Rigid retaining walls with narrow cohesionless backfills under various wall movement modes. Int. J. Geomech., 10.1061/(ASCE)GM.1943-5622.0001007, 04017098

[30] Spangler, M.G., & Handy, R. L. (1982). Soil Engineering, Harper & Row, New York.

[31] Khosravi, M. H., Pipatpongsa, T., & Takemura, J. (2016). Theoretical analysis of earth pressure against rigid retaining walls under translation mode. Soils Found., 56(4), 664-675.